Experimental simulation of rolling–sliding contact for application to planetary roller screw mechanism

G. Aurégan [a,b,*], V. Fridrici [a], Ph. Kapsa [a], F. Rodrigues [b]

[a] Laboratoire de Tribologie et Dynamique des Systèmes, UMR CNRS 5513 ECL-ENISE, Ecole Centrale de Lyon, Bat. H10, 36 Avenue Guy de Collongue, 69134 Ecully Cedex, France
[b] Messier-Bugatti-Dowty, SAFRAN Group, France

ABSTRACT

The planetary roller screw mechanism is used in the aeronautics industry for electro-mechanical actuators application. It transforms a rotational movement into a translation movement, and it is designed for heavy loads. The main components are made of martensitic stainless steel, and lubricated with grease. Like most usual rolling mechanisms, smearing and jamming can occur before the theoretical fatigue lifetime, especially in defective lubrication conditions.

The actuated load is carried by small contacts between the threads of the screw, the rollers and the nut. The static single contact can be described as an ellipsoid on flat contact; motion consists of rolling with sliding perpendicular to the rolling direction. A calculation method based on elastic theories (Hertz, Carter, Johnson) has been implemented. It calculates the normal and tangential stresses distributions, generated in the micro-slip and stick zones of the contact area, using several input parameters such as material properties, normal force, and creep ratio.

A specific apparatus has been developed to support these calculations and to experimentally study the damage of the contacts in this mechanism. It consists of a freely rolling wheel loaded on a rotating disc with a component of sliding that simulates the roller screw contact. The tribometer inputs are the normal load, the speed, the creep ratio, and the lubrication. The wheel rolling speed and the tangential force generated in the direction perpendicular to rolling are measured.

The experiments reveal a quick adhesive wear in dry or bad lubricated conditions, while a low friction coefficient remains if the contact is well lubricated. The influence of the input parameters concurs with the theoretical calculation. The evolution of grease lubrication during duty lifetime and the influence of the tribo-chemical films on this lifetime are also studied.

© 2015 Elsevier B.V. All rights reserved.

1. Introduction

The planetary roller screw (PRS) is a device that converts rotation to translation motion or vice versa. This mechanism includes rollers between the screw and the nut to limit friction (Fig. 1). The basic principle is similar to the ball screw mechanism, but it is designed for high speed and long life applications. Especially, the rollers threads increase the contact surface and then allow carrying heavier loads for a relatively small external diameter. These features make the PRS attractive for aeronautics electro-mechanical actuators that must be small sized and highly stressed.

The lifetime calculation of this component is based on fatigue failure like most bearing mechanisms. However, it is known that

bearing parts made of stainless steel often fail long before the calculated time, because of other failure modes such as adhesive wear [1]. Smearing damage is closely linked to the lubrication conditions and the contact stresses, and is complicated to predict. Also, the design of PRS is quite different from usual rolling components, and includes rolling–sliding motion and parasite forces that can drastically influence the lifetime.

Despite its importance in many application fields such as manufacturing and robotics, the use of the PRS never required a high level of reliability in high stress conditions. Then, very few fundamental researches have been performed to improve the design and the lifetime calculation. Yet, as the PRS becomes interesting for critical application like actuators for the aeronautics, some work has been made in recent years to better understand its kinematics [2–7].

The present work investigates the tribological behavior of the PRS mechanism. The objective is to study the influence of the contact parameters to provide information on smearing occurrence. Results should provide tools to predict the hazardous configurations and

* Corresponding author at: Laboratoire de Tribologie et Dynamique des Systèmes, UMR CNRS 5513 ECL-ENISE, Ecole Centrale de Lyon, Bat. H10, 36 Avenue Guy de Collongue, 69134 Ecully Cedex, France. Tel.: +33 47218 6025; fax: +33 47843 3383.

E-mail address: gilles.auregan@ec-lyon.fr (G. Aurégan).

Nomenclature

i	screw, nut or roller
F_{tot}	axial load on a single contact (N)=total axial load/number of contact points
F_n	normal force (N) $= F_{tot}/\cos\beta$
F_t	tangential friction force (N)
R_{curv}	radius of curvature of the roller profile (mm)
R_i	pitch radius of the component i (mm)
R	radius of the track on the disc (mm)
τ	creep ratio $(=V_{sliding}/V_{rolling}=\tan\Theta)$
Δ	axial shift on the test rig
Θ	creep angle (°)

p_i	pitch of the component i (mm)
α_i	helix angle of the component i (°)
β	tilt angle (°) generally equal to 45°
$V_{rolling}$	in-plane rolling speed of the PRS roller (m s^{-1})
$V_{sliding}$	in-plane sliding speed of the PRS contact (m s^{-1})
$V_{ax.sliding}$	axial sliding speed of the PRS contact (m s^{-1})
V_{disc}	speed of the contact point on the disc (m s^{-1})
$v_{rolling}$	speed of the contact point on the roller (m s^{-1})
$v_{sliding}$	sliding speed of the roller sample (m s^{-1})
p_o	maximum Hertz pressure (MPa)
p	local normal stress (MPa)
q	local shear stress (MPa)
μ	friction coefficient $(=F_t/F_n)$

---

increase the reliability. First, a theoretical analysis of the contact conditions has been made. Second, a calculation method has been implemented to calculate the contact features such as slide/roll ratios, stresses and stick/slip zones distribution, in order to evaluate its susceptibility to smearing. Then, a specific tribometer that reproduces the RPS contact is presented. Rolling–sliding wear tests were performed with different working conditions such as speed, creep ratio, and lubrication. Wear tracks and forces measurement data are analyzed.

2. Mechanical and tribological features of the contact

2.1. Static description of the contact

The PRS consists of a screw and a threaded nut of the same pitch (Fig. 1), with rollers in between. The thread profile of the screw and the nut is straight and usually cut to 90° for best efficiency. Threaded rollers are set between the two components, and their profile is curved to further reduce friction. The axial load is transmitted through multiple contacts between the threaded components. Then, these contacts can be described as ellipsoid-on-flat contacts (Fig. 2) that are characterized by three radii: the pitch radius of the screw (or the nut) and the roller, and the roller's radius of curvature. They are subjected to a single normal force F_n that is the 45° projection of the single axial load F_{tot}. The resulting contact area is an ellipse whose characteristics can be calculated using the Hertz theory. For unique loading direction, only one side of the thread works because of axial backlash.

2.2. Dynamic features

The overall motion is similar to that of an epicyclic gear train: the rotation of the screw drives the orbital motion of the rollers. The rollers are synchronized with spur gears at their ends and ring gears at the ends of the nut. The rollers threads are rolling on those of the nut and the screw.
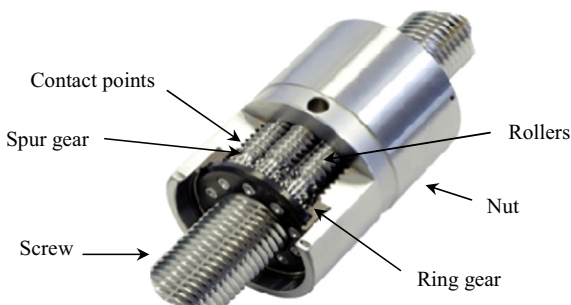
$$p_{nut} = p_{screw} \tag{1}$$

$$R_{nut} = R_{screw} + 2 \times R_{roller} \tag{2}$$

$$p_i = \pi \times R_i \times \tan\alpha_i \tag{3}$$

$$\alpha_{nut} = \alpha_{roller} \tag{4}$$

$$\alpha_{screw} \neq \alpha_{roller} \tag{5}$$

Since the nut and the screw have the same pitch (Eq. (1)) and different diameters in order to house the rollers (Eq. (2)), their two threads have different helix angles (Eq. (3)). Besides, the rollers must have the same helix angle as the nut to prevent them from axial migration as they roll into the nut (Eq. (4)) [3]. Thus, the roller helix angle cannot also be equal to that of the screw (Eq. (5)).

This difference results in an overall axial sliding component, and thus a slip ratio (also called creep ratio τ) of the single contact, perpendicular to the rolling direction, and given by

$$\tau = \frac{V_{sliding}}{V_{rolling}} \tag{6}$$

A complete analysis of the PRS is provided by Velinsky et al. [3]. This approach gives the global axial sliding speed considering the angular speed of the screw

$$V_{ax.\,sliding} = R_{screw}\omega_{screw}\tan\alpha_{screw} \tag{7}$$

where ω_{screw} is the angular speed of the screw. For tribology matters, it is interesting to express the sliding speed as the product of a rolling speed and a slip ratio, since these two parameters are related to thermal effects and sliding amplitude.

The rolling speed is defined as the angular speed of the rollers as they roll on the screw profile. It is calculated as [3]

$$V_{rolling} = \frac{R_{screw} + 2R_{roller}}{2(R_{screw} + R_{roller})}R_{screw}\omega_{screw} \tag{8}$$

The creep ratio can be calculated by considering the gap between the helix angle of the screw, and the helix angle of the rollers which is generally oriented in the opposite direction. Fig. 3 illustrates this gap with exaggerated angles.

The rollers move in the orbital direction at the speed of $V_{rolling}$. To stay on the screw pitch line, the contact must slide in the axial direction at the speed of

$$V_{ax.sliding} = V_{rolling}(\tan\alpha_{screw} + \tan\alpha_{roller}) \tag{9}$$

Due to PRS geometry characteristics, this expression (Eq. (9)) gives the same results as the previous expression of $V_{ax.sliding}$ (Eq. (7)).
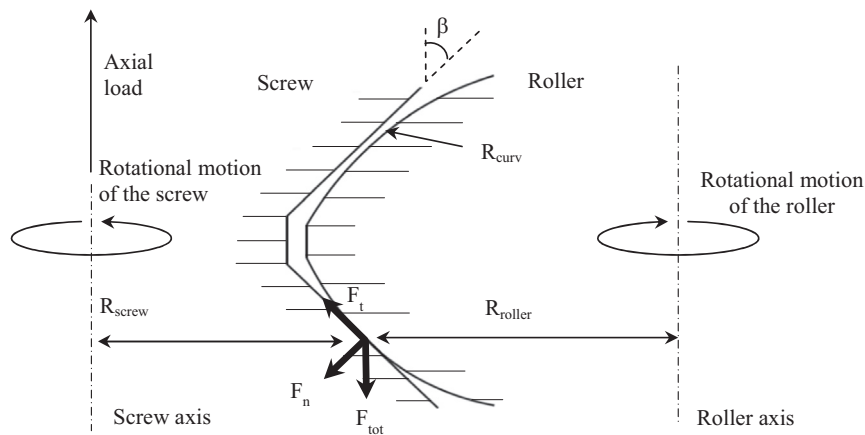

Fig. 1. PRS main components.

Contact points

Spur gear

Rollers

Nut

Screw

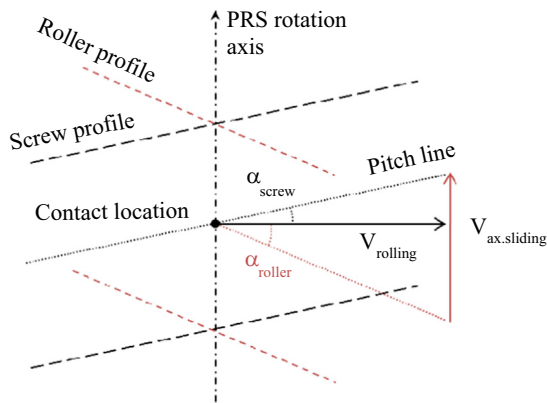Ring gear

Fig. 2. Single contact features.

Fig. 3. Axial schematic view of the PRS contact.

Since the contacting threads are tilted from the axis to an angle β, the actual sliding speed at the contact point and the creep ratio are (cf. Fig. 2).

$$V_{sliding} = V_{rolling}(\tan \alpha_{screw} + \tan \alpha_{roller})\cos \beta \quad (10)$$

$$\tau = \frac{V_{sliding}}{V_{rolling}} = (\tan \alpha_{screw} + \tan \alpha_{roller})\cos \beta \quad (11)$$

The creep ratio and the rolling speed are directly related to the PRS design: for small pitches PRS, helix angles are smaller than for large pitches PRS, but applied speeds are usually higher. Then, the wear behavior would be different from one design to another. Typically, the creep may vary from 5% to 10%.

Finally, since the contact is not punctual and is tilted from the rotation axis, the constant sliding lines inside the contact describe a class of circles whose centers may or may not lie within the contact area. This phenomenon is referred to as spin [8]. In the small pitch PRS considered in the present study, the width of the contact area is negligible compared to the pitch radius, so that the sliding lines can be considered parallel, and the spin effect is neglected.

Some orbital sliding can also occur when there is a pitch mismatch between the gears and the thread. It results in a slight axial migration of the rollers [2]. This component is due to manufacturing errors, and is not discussed in this paper. Finally, slip can also arise due to the difference between the two surfaces curvatures. It has been suggested that this micro-slip can be sufficient to generate adhesive wear and being responsible for the rolling resisting moment [1,8].

The single contacts that carry the load in the PRS can be described as ellipsoid on flat contacts, with a rolling–sliding motion. Since the spin effect due to the tilted contact is second order, they can be assimilated to a more common rolling contact with rotation axis parallel to the contact area, and subjected to the normal load F_n.

Thus, it is similar to the wheel/rail contact or gear tooth contact [9,10], but with a sliding motion perpendicular to the rolling direction [11,12].

2.3. Presentation of the calculation method

Tribological behavior is closely related to the contact ellipse features, such as the shear stress distribution. The study of the PRS simplified contact area may give information about the wear lifetime of the mechanism.

Sliding–rolling contacts have been widely studied for bearings and gears [1,13,14]. Sliding can arise from speed differential between the rolling elements, or from a difference of curvatures like in the spherical roller thrust bearings [15]. Generally speaking, wear related to slip components arises in poor lubrication conditions, when the metallic parts are directly in contact. Sliding–rolling contacts are also studied for railways application where the speed difference between the wheel and the rail generates traction.

For complete slip of the contact area, the tangential stresses at the bodies' surfaces are easy to calculate. But, for small creep ratios, the two bodies may not be entirely slipping. Theories have been developed to take into account the materials elastic compliance. Carter [16] treated the 2D problem of the tractive rolling of elastic cylinders: the total shear stress is calculated by addition of the shear stresses for complete slip and complete stick at the leading edge of the contact (Fig. 4).

For sufficiently small creep ratios, the contact area is divided into slip and stick areas. For higher speed differences, the contact is in complete slip. The different configurations of stick and slip are presented on a typical traction curve (Fig. 5), which represents the evolution of the tractive tangential force versus the creep ratio τ.

Later, the theory was extended to 3D contacts by Johnson [8], Haines et al., and Kalker [17] who developed algorithms based on these theories for wheel–rail contact application.

The basic principle of the 3D theory is to decompose the contact into thin strips and to apply the Carter theory to each of these strips. For dry tractive rolling, the stick zone of the contact area usually vanishes for creepage under 10%. In PRS, the creep ratio is typically of this order of magnitude. Then it is necessary to take into account these theories to study the PRS contact behavior.

The strip theory can also be used to calculate the shear stress and slip regions due to rolling micro-slip in pure rolling motion [8]. In that case, the creep ratio only depends on the curvatures of the two bodies. Related experiments have shown that the contact is divided into three slip zones of opposite direction, and two no-slip lines.
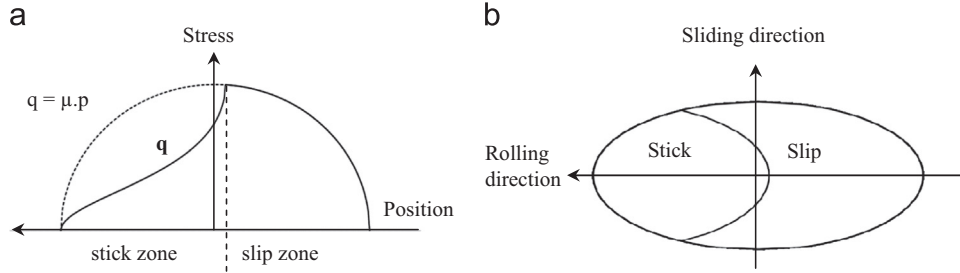
Fig. 4. Stick/slip distribution in the contact ellipse. (a) Stress distribution over the main ellipse axis, and (b) top view of the contact ellipse.
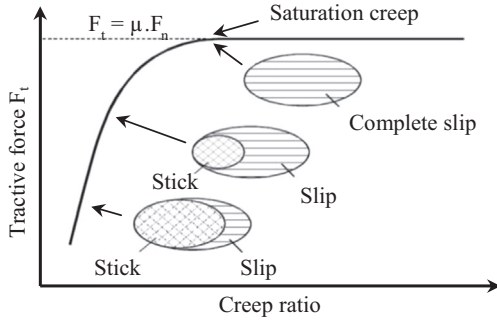

Fig. 5. Typical traction curve.

A method based on the 3D strip theory has been implemented to calculate the shear stresses and stick/slip distribution in an ellipsoid on flat contact, for several input configurations:

– Static features are calculated with the Hertz theory. The input parameters are the radius of curvature R_{curv} and the pitch radius R_{roller} of the roller, the pitch radius of the screw R_{screw}, the normal load (F_n), and the material elastic properties. The output parameters are the result of Hertz calculations: contact pressure distribution, indentation depth, and size of the contact ellipse.
– Dynamics sliding features related to transverse slip and pure rolling micro-slip are calculated separately: for transverse sliding, the inputs are the Hertz theory results, the friction coefficient, and the creep ratio τ deducted from the helix angles (cf. Section 2.2). As outputs, the method gives the percentage of stick and slip within the contact, then calculates the generated tangential force F_t, and gives graphical distribution of stick/slip zones. It also draws a traction curve that gives the saturation creepage for a given contact configuration. For the pure rolling micro-slip, the only inputs are the Hertz theory results, the friction coefficient and the radius of curvature.

For both sliding types, the program also drafts a 2D illustration of the shear stress evolution along the central strip, which gives the value of the maximum shear stress inside the contact.

2.4. Results and discussions

2.4.1. Traction curves
The method gives the evolution of the saturation creep ratio for various normal loads and friction coefficients. It uses the simple carter 2D expression of creep that applies for two elastically similar bodies transmitting a lateral tangential force F_t [8]

$$\tau = \frac{2\mu p_o}{G}\left\{1 - \left(1 - \frac{F_t}{\mu F_n}\right)^{\frac{1}{2}}\right\} \tag{12}$$

where G is the shear modulus. Fig. 6a shows the evolution of $F_t/\mu F_n$ for a friction coefficient of 0.5 and various values of F_n typical of

bearing parts. It reveals that higher normal forces allow greater tangential strains before the complete slip, and then higher saturation creep. Similarly, it also reveals that for the same value of normal force, the contact will slip more easily for small friction coefficients (Fig. 6b). In both cases, it appears that complete slip occurrence strongly depends on contact parameters. Regarding wear behavior, it is likely that adhesive micro-welding arises more easily in complete slip motion rather than in partial slip.

2.4.2. Maximum shear stress
If the slip zone matches the most stressed zones of the contact, it is likely that adhesive wear occurrence will be higher. The slip zones are always at the trailing edge of the rolling contact. In this area, the shear stress q matches the complete slip curve, thus q is equal to μp from the beginning of slip until the contact exit. As p becomes small at the edges of the contact (Hertz pressure distribution), little slip zones are not likely to generate much wear. For larger slip zones i.e. higher τ (Fig. 7), the surface may start to slip in the middle of the contact where the normal pressure p is higher, which could be more critical regarding smearing. Hence, the best configuration would be to maximize the tangential strain in order to reduce the slip zone magnitude.

2.4.3. Calculation of rolling friction micro-slip
The rolling micro-slip arises from the curvatures of the roller profile (Fig. 8). Then, if the tangential stress generated is significant, the contact would be an association of transverse sliding and rolling microslip. The calculation sheet can meet the two components separately on the same draft, in order to compare the stress they generate. For dry contact condition ($\mu \sim 0.8$), the three microslip zones are very small and located near the contact edges. Then, the maximum shear stress is also very low.

Thus, for creep ratios around 0.01–0.05 the rolling microslip shear stress is negligible compared to that of the transverse sliding. But for lower creep ratios ($\tau < 0.01$), rolling friction becomes significant. Besides, the magnitude of rolling micro-slip is related to the width of the contact area: for larger contact width, the speed difference between the middle and the edges will be greater. In particular, considering the high normal stress the threads may undergo, a slight plastic groove may be formed, that could increase the rolling friction [8].

This calculation method is suitable for any contact configurations, and gives important results such as normal pressure, mean and maximum shear stresses, stick/slip distribution, and resisting moments. It reveals that the stick magnitude in the contact is strongly dependent on the creep ratio, and varies greatly with the normal pressure and the lubrication condition. For significant creep ratios, the rolling friction is negligible compared to the overall transverse sliding.
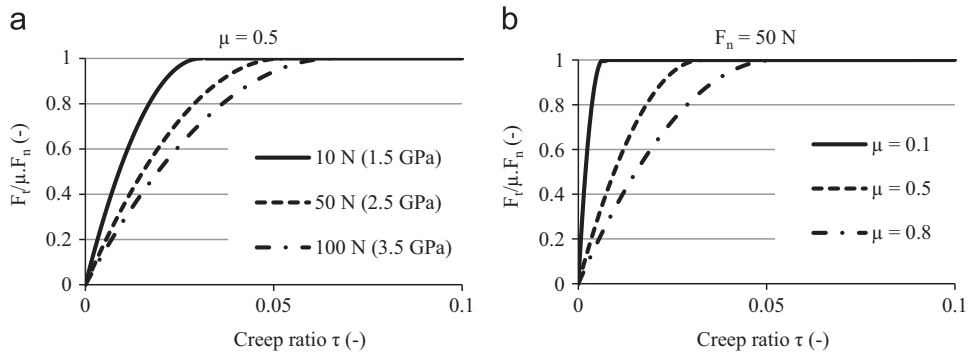
Fig. 6. Evolution of traction curves with normal load and friction coefficient. (a) $\mu=0.5$ various F_n, and (b) $F_n=50$ N, ($p_o=2.5$ GPa) various friction coefficients.
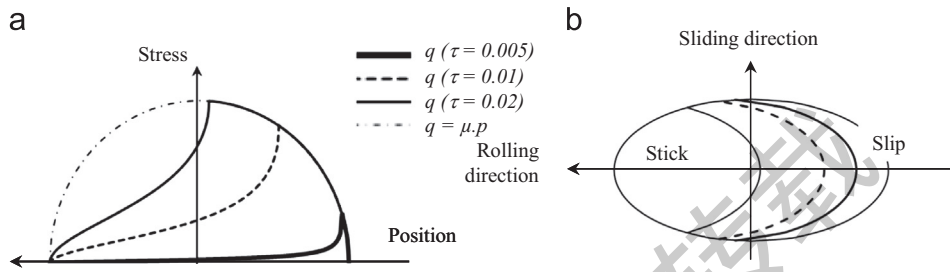

Fig. 7. Evolution of maximum shear stress and stick/slip distribution for various creep ratios. (a) Stress distribution over the main ellipse axis, and (b) top view corresponding stick/slip zones delimitation.
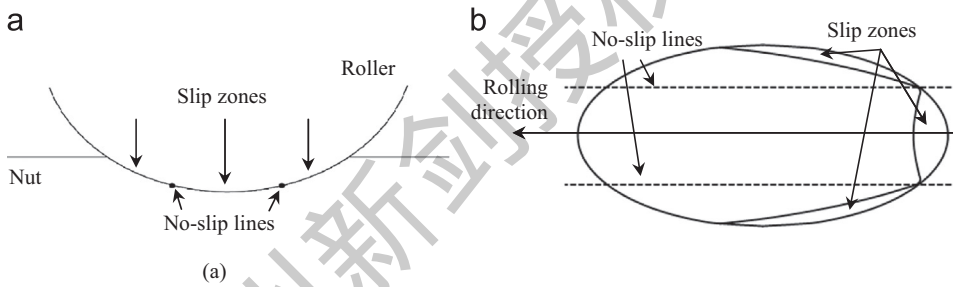

Fig. 8. Rolling friction due to micro-slip in pure rolling motion. (a) Front view of the rolling contact, and (b) top view of the contact ellipse.
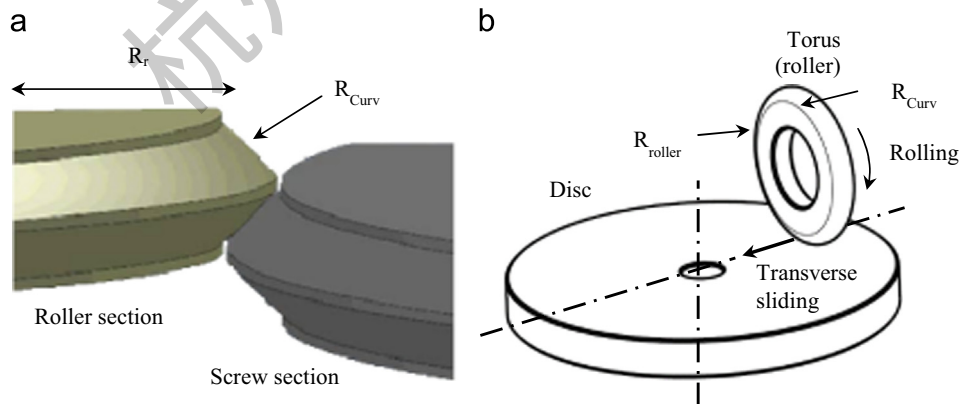

Fig. 9. Configuration of the simulated contact. (a) PRS screw/roller contact, and (b) test rig contact.

Table 1
Chemical composition of samples materials.

|	C	Si	Mn	S	P	Ni	Cr	Mo	V	Fe	N_2	Cu
Disc	0.426	0.26	0.37	< 0.0015	0.016	< 0.30	15.68	1.82	0.29	Compl.	0.20	–
Roller	0.984	0.41	0.46	< 0.0015	0.015	0.21	17.69	0.44	–	Compl	–	–

3. Experimental details

3.1. Samples and materials

The PRS single contact is difficult to reproduce experimentally. But it can be reasonably assimilated to the contact of a curved body on a flat surface, with rolling and sliding. A test rig has been developed to simulate this simplified configuration and then study the damage induced by the rolling–sliding motion. It uses a torus and a flat disc as samples (Fig. 9), which represent respectively the roller and the screw profiles. A given PRS of small pitch (p_{screw}=2.5 mm) has been chosen as a reference for the design of the two specimens. The aim is to obtain the same characteristics of contact: ellipse size and contact pressure for a given load, same materials and lubrication.

The external radius of the torus is 10 mm. It corresponds to the pitch radius R_r of the PRS roller. The radius of curvature is set to be 1.5 mm, equal to the roller curved profile. The materials are martensitic stainless steels similar to those of the PRS components. Tables 1 and 2 present the chemical composition and their mechanical properties. Surfaces are grinded to obtain Ra ≈ 0.15 μm. Some samples are also polished (Ra < 0.005 μm). Some experiments will be made in presence

Table 2
Mechanical properties of samples materials.

	Rm (MPa)	Hardness (HRc)	Young modulus (MPa)	Poisson coefficient
Disc	2500	≥ 58	210×10^3	0.3
Roller	2350	≥ 58	210×10^3	0.3
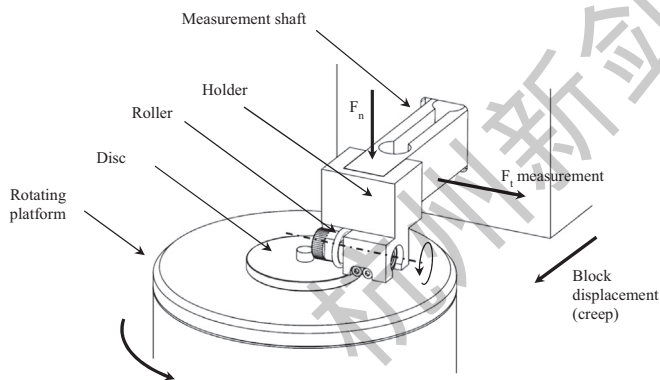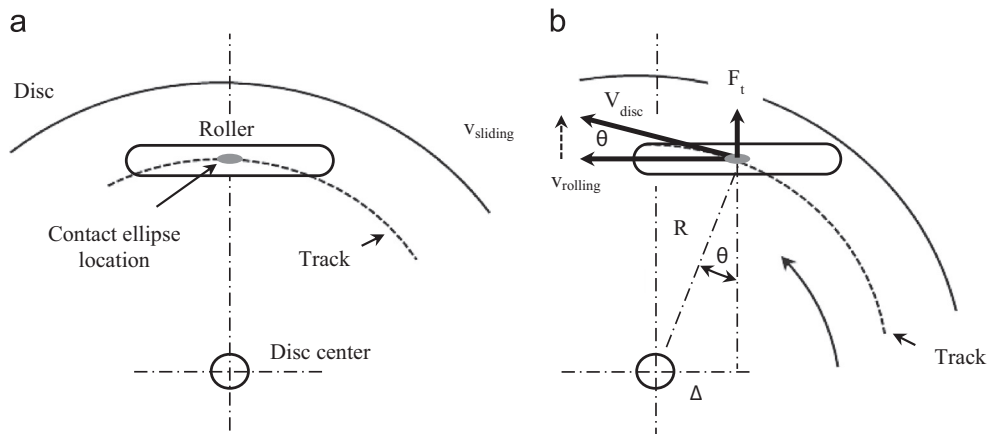
of the grease generally used for PRS. It is thickened with *Microgel*® and it contains anti-wear and high-pressure additives.

3.2. Rolling–sliding tribometer

A specific test rig has been developed to reproduce the PRS kinematics. The roller is mounted on a small shaft that rolls freely on small ball bearings inside a holder. The holder is fixed to a shaft that loads the assembly on the rotating disc (Fig. 10). Tangential force and rolling speed are measured and recorded. The transverse sliding component is generated by moving the contact perpendicularly to the radius of the disc (Fig. 11).

The axial shift Δ between the roller axis and the disc axis is controlled with precision and creates a radial sliding component. As a result, it generates a tangential force F_t.

The creep ratio τ is defined by $\tau = (V_{sliding}/V_{rolling}) = \tan \theta$.

Hence Δ is calculated as follows: $\Delta = R \sin \theta = R \sin (a \tan \tau)$, where R is the radius of track on the disc.

3.3. Test conditions

First, the test rig can be used to plot continuous traction curve by varying the axial shift Δ during one single test. Then, wear tests can be conducted with continuous or alternative rotation to reproduce the PRS contact kinematics. Table 3 summarizes the wear test conditions of the roller–disk contact on the tribometer, in order to simulate one single contact between the roller and the screw in the PRS. All tests are performed at room temperature (22 °C).

4. Experimental results and discussions

4.1. Traction curves

Traction curves have been performed for two different lubrication conditions and the same normal load. Fig. 12 shows typical results for lubricated and dry conditions. They are compared to the theoretical curves from Section 2.4 calculated for the geometry of the roller–disk contact of the test rig.

It appears that, for lubricated contact, the partial slip part of the experimental curve follows the theoretical calculation. After the inflection point which corresponds to the transition from partial slip to complete slip, the tractive force increases slightly before joining the μF_n limit. This evolution can be related to the structure of the lubricant: the grease shear modulus is higher than for the oil; thus it needs to be more sheared to reach the base oil friction coefficient. The performed curve reveals that when lubricated, the

Fig. 10. Tribometer.

Fig. 11. Generation of the transverse sliding component. (a) Top view of pure rolling position $\Delta=0$. (b) Top view of rolling–sliding position $\Delta \neq 0$.

contact starts to slip for very small creep ratios ($\tau < 0.01$). For most PRS, the helix angles creep is about 0.02, so we can expect that the PRS contact will always be in complete slip when lubrication is efficient.

The dry contact traction curve does not fit the calculation as well. Contrary to the lubricated condition, the tangential force is strongly dependent on the surface condition that evolves quickly during the test because of adhesive wear. A multiple tests plot would be more appropriate.

4.2. Unlubricated wear tests

Real PRS are used with grease; but because of their kinematics, the grease can sometimes not be present in the contact, leading to a global failure. Thus, the dry wear tests must give information about the tribological behavior in case of lubrication failure. For these experiments, the samples are polished and cleaned. Several test conditions have been tested (Table 3). The typical evolution of the friction coefficient is presented in Fig. 13 for conditions representative of a real PRS. One cycle is defined as one rotation of the disc. The F_t/F_n ratio increases quickly from 0.1 to 0.4, and then stabilizes at 0.5. Several tests have been performed and stopped after different numbers of cycles to observe the damaged surface. The optical observations reveal transfers of material typical of adhesive wear. These smearing zones are first scattered (Fig. 14a) in the middle of the track (maximum stresses), and then grow in the direction of creep i.e. perpendicular to the rolling track (Fig. 14b). As F_t/F_n reaches 0.5, pictures reveal a severe wear and higher materials transfers. At this point, the wear scar is not symmetrical to the middle of the track and shows a gradient in the direction of sliding (Fig. 14c). The relation with the stick/slip theoretical distribution is tricky though.

These results are very different from classic pure sliding tests because the rolling component influences the wear mechanisms in several ways: it flattens the adhesive transfer at each cycle and it reduces the instantaneous sliding amplitude of the slipping surfaces. Anyway, in dry test conditions, smearing occurs extremely quickly. Also, other wear tests revealed that adhesive wear even happens for lighter conditions (F_n down to 2 N).

A special case arises for pure rolling motion ($\tau = 0$). Observations reveal that smearing even occur without transverse creep (Fig. 15). The wear track is strip shaped along the rolling direction. That observation is directly related to the existence of slip bands due to roller's curvature (Fig. 8).

These observations show that the wear pattern is similar to that of the usual bearing parts: without lubrication, smearing quickly arises from the micro-slip zones. This results in a progressive transfer of small particles from both surfaces. These transfer patches grow at each cycle and lead to the global degradation of the track. Besides, the PRS contact geometry seems more hazardous than usual bearings because of the transverse sliding component. Lastly, the curvature of the roller influences the contact width and then the rolling micro-slip zones.

4.3. Lubricated wear tests

In practice, it is unlikely that the lubrication breaks down suddenly and leaves cleaned and dry surfaces in contact. However, it is common that the quantity of grease may become insufficient to properly separate the contacting surfaces. Works have been made [1,15] to understand the evolution of lubrication regimes during the bearings lifetime. Most of these studies deal with oil lubrication, but some researches have been treating with the grease behavior [18]. It appears that grease lubrication involves several stages before it becomes too poor to prevent surfaces from smearing [19]. For first cycles, the grease film is thick enough to provide hydrodynamic and E.H.D regimes that totally separate the rolling bodies. As the grease spreads around the contact, the regime switches to boundary. At this stage, contacts between asperities occur and tribo-chemical reactions with the additives may take place to generate a protective tribofilm.

Table 3
Test conditions and contact parameters.

Normal load, F_n	50–100 N
Maximum Hertz pressure	1500–3500 MPa
Ellipse size	$a = 0.4$–0.5 mm, $b = 0.1$–0.15 mm
Creep ratio, τ	0–10 %
Contact rolling speed	500–2000 mm s^{-1}
Lubrication	Dry cleaned surface/greased surface
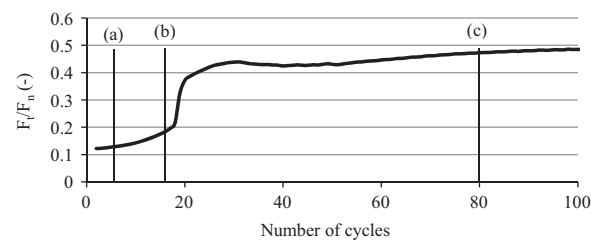
Fig. 13. Typical evolution of F_t/F_n for dry test conditions. $F_n = 80$ N ($p_o = 3000$ MPa), $V_{rolling} = 1$ m s^{-1}, and $\tau = 0.015$. (a) 10 cycles, (b) 20 cycles, and (c) 80 cycles.
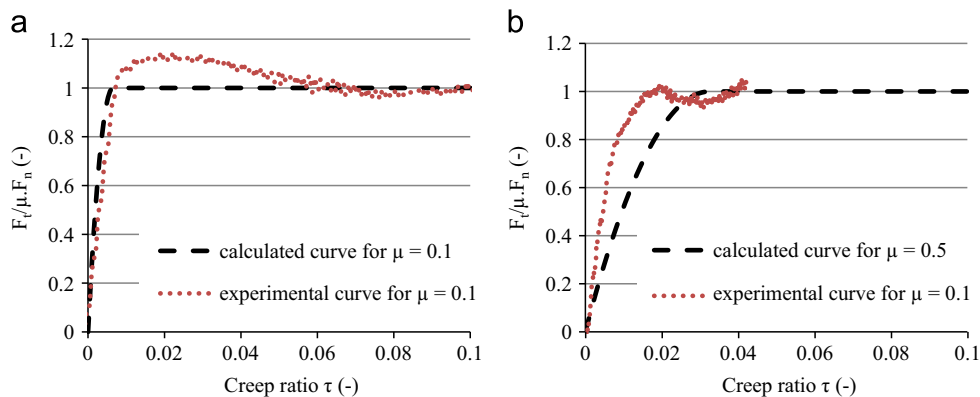
Fig. 12. Experimental and calculated traction curves for $F_n = 50$ N. (a) Lubricated contact, and (b) dry contact.
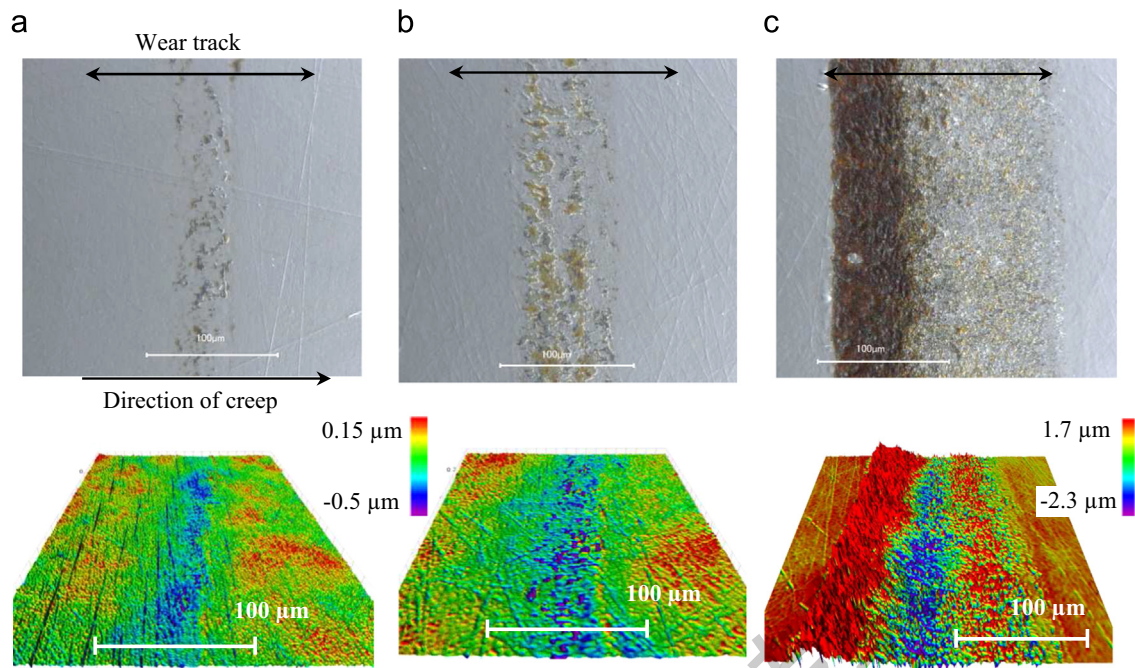
Fig. 14. Optical and interferometry observation of the test track (disc) for 3 numbers of cycles (a–c) (see Fig. 13).
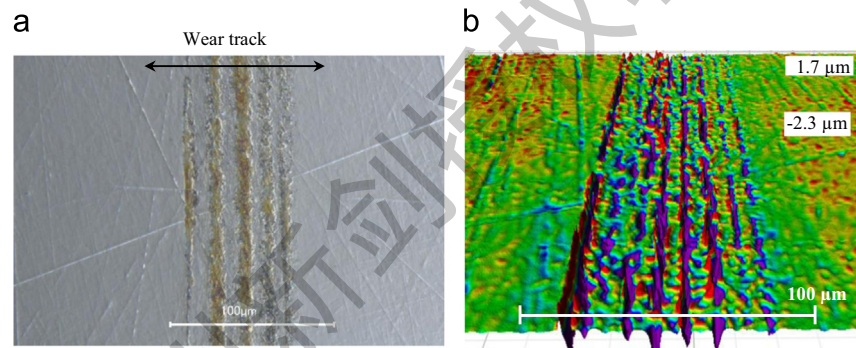

Fig. 15. Optical and interferometry observation of the track (disc). $F_n = 5$ N, $V_{rolling} = 0.5$ m s^{-1}, $\tau = 0$ (pure rolling motion), dry condition.

These studies reveal that the starvation regime can appear very quickly during the first cycles, and that wear lifetime is usually governed by tribo-chemical phenomena [18,19].

Lubricated wear tests have been performed on the rolling–sliding test rig. These experiments involve a new parameter that is the initial grease thickness deposited on the disc before the test.

4.3.1. Large initial grease thickness

Long duration tests (20 h) have been performed with high stresses, speeds and creep ratios to evaluate the tribological behavior in extreme conditions when the contact is well lubricated. The friction coefficient stabilizes around 0.12 (Fig. 16) during the whole test. Fig. 17a shows the presence of a tribo-chemical film on worn surfaces. XPS analysis revealed that zinc compound is found in the grease and in the tribofilm, which reveals the presence of usual EP additives such as ZnDDP [20]. Its distribution is not homogenous on the wear track. Darker colors are usually related to different chemical products [21], and thus to more stressed areas. Therefore, observations confirm the theoretical dissymmetric stress distribution due to creep. Lastly, the same test performed without creep (Fig. 17b) reveals a much lighter quantity of tribochemical film. This is due to density of asperities in contact that is necessarily lower without a sliding component.
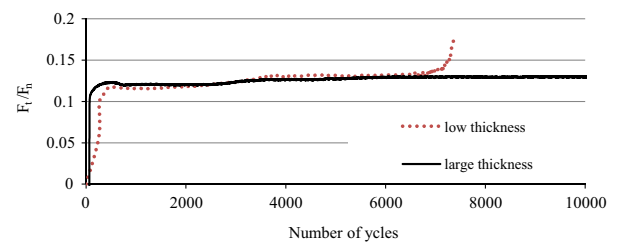

Fig. 16. Evolution of friction coefficient for small and large thickness of grease. $F_n = 80$ N, $V_{rolling} = 1$ m s^{-1}, $\tau = 0.015$.

Besides, the picture also reveals a tribofilm distribution divided into three darker bands on the middle and on the edges, that corroborates the theoretical analysis (Fig. 8).

4.3.2. Low initial grease thickness

Low grease thickness tests have been performed to reproduce the situation of insufficient lubrication that may occur in the PRS mechanism. Fig. 16 shows the comparison of F_t/F_n between small and large grease thickness. The evolution of F_t/F_n first fits the large thickness one, and then raises quickly after a certain number of cycles that varies from one test to another.
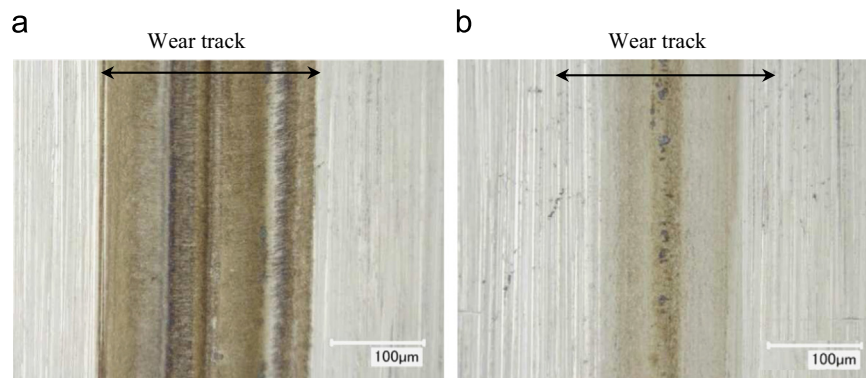
Fig. 17. Optical observations of the wear track (disc) for large grease thickness tests. $F_n = 130$ N, $V_{rolling} = 2$ m s^{-1}, 20 h ($\sim 10^6$ cycles). (a) $\tau = 0.04$, and (b) $\tau = 0$.

These results show that a very slight difference in initial grease thickness can significantly influence the smearing lifetime. Besides, they also reveal that adhesive wear occurrence is also strongly influenced by rolling speed and normal load. Generally speaking, it appears that a starved regime occurs very quickly, especially for high pressure and high rolling-speed. Thus, the tribochemical reactions also arise quickly, and the high or low friction behavior is provided by a competition between destruction and creation of the tribofilm [22]. As these reactions are closely related to the additives flow under the contact, it is likely that if the initial grease thickness is too low, and if stresses and speed are too high, the additives density will not be enough to provide a sufficient protective film.

5. Conclusions

This work investigates the tribological behavior of the contact at the screw/roller and nut/roller interfaces of the PRS mechanism.

A simple analysis that describes the contact characteristics has been provided. As a result, the contact can be considered as an ellipsoid on flat contact with a rolling component, and a sliding component perpendicular to the rolling direction. This makes the PRS contact much singular among usual bearing mechanisms. The contact parameters such as normal load, rolling speed and slip ratio are derived.

A method has been implemented to calculate the contact features such as tangential stress distribution, and stick/slip distribution. It reveals that complete slip may occur for relatively small creep ratios, and that consequently the screw/roller contacts may always be entirely slipping. Thus, the creep ratio may have a detrimental influence on the adhesive wear lifetime.

A specific apparatus has been developed to reproduce the simplified PRS contact features: it simulates the screw/roller and nut/roller interfaces with a torus roller rolling and sliding on a disc. Input parameters such as normal load, rolling speed and creep ratio are controlled, so that the static and dynamic features of the contact ellipse in the laboratory test are representative of the contact in one reference PRS used in industry. Tests have been performed in both lubricated and dry conditions. It reveals that without lubrication, the contact smears very quickly even in low stress conditions, and that rolling micro-slip due to curvature is sufficient to generate smearing. On the contrary, when lubricated with large grease thickness, the contact does not show any adhesive wear after more than 10^6 cycles. However, the tracks observation shows important tribo-chemical layer which is created quite early during the tests. Other tests with variable initial grease thickness reveal that, for insufficient grease quantity, the starved regime cannot stabilize and smearing occurs quickly.

This work shows that the PRS mechanism features some unusual parameters, that evolve from one design to another, and which are very likely to influence the tribological behavior. In particular, the magnitude of the transverse slip ratio and rolling speed are directly related to quick smearing when lubrication becomes insufficient. Besides, these parameters are also likely to promote the generation of a protective layer which can stand for many cycles when starved lubrication occur.

References

[1] J. Halme, P. Andersson, Rolling contact fatigue and wear fundamentals for rolling bearing diagnostics – state of the art, Proc. Inst. Mech. Eng. J: J. Eng. Tribol. 224 (4) (2010) 377–393.
[2] M.H. Jones, S.A. Velinsky, Kinematics of roller migration in the planetary roller screw mechanism, J. Mech. Des. 134 (6) (2012).
[3] S.A. Velinsky, B. Chu, T.A. Lasky, Kinematics and efficiency analysis of the planetary roller screw mechanism, J. Mech. Des. 131 (1) (2009).
[4] M.H. Jones, S.A. Velinsky, Contact kinematics in the roller screw mechanism, J. Mech. Des. 135 (5) (2013).
[5] Y. Hojjat, M. Mahdi Agheli, A comprehensive study on capabilities and limitations of roller-screw with emphasis on slip tendency, Mech. Mach. Theory 44 (10) (2009) 1887–1899.
[6] S. Ma, G. Liu, R. Tong, X. Zhang, A new study on the parameter relationships of planetary roller screws, Math. Probl. Eng. 2012 (2012).
[7] P.A. Sokolov, D.S. Blinov, O.A. Ryakhovskii, E.E. Ochkasov, A.Y. Drobizheva, Promising rotation–translation converters, Russ. Eng. Res. 28 (10) (2008) 949–956.
[8] K.L. Johnson, Contact Mechanics, Cambridge University Press, Cambridge, UK, 1987.
[9] J. Ayasse, H. Chollet, Wheel–rail contact, in: S. Iwnicki (Ed.), Handbook of Railway Vehicle Dynamics, CRC Press, Boca Raton, FL, USA, 2006.
[10] U. Olofsson, R. Lewis, Tribology of the wheel–rail contact, in: S. Iwnicki (Ed.), Handbook of Railway Vehicle Dynamics, CRC Press, Boca Raton, FL, USA, 2006.
[11] A.D. Monk-Steel, D.J. Thompson, F.G. de Beer, M.H.A. Janssens, An investigation into the influence of longitudinal creepage on railway squeal noise due to lateral creepage, J. Sound Vib. 293 (3–5) (2006) 766–776.
[12] D. Thompson, C. Jones, Noise and Vibration from Railway Vehicles, in: S. Iwnicki (Ed.), Handbook of Railway Vehicle Dynamics, CRC Press, Boca Raton, FL, USA, 2006.
[13] R. Evans, T. Barr, L. Houpert, S. Boyd, Prevention of smearing damage in cylindrical roller bearings, Tribol. Trans. 56 (5) (2013) 703–716.
[14] K.L. Johnson, The effect of a tangential contact force upon the rolling motion of an elastic sphere on a plane, J. Appl. Mech. 80 (1958) 339–346.
[15] U. Olofsson, S. Andersson, S. Björklund, Simulation of mild wear in boundary lubricated spherical roller thrust bearings, Wear 241 (2) (2000) 180–185.
[16] F.W. Carter, On the action of a locomotive driving wheel, Proc. R. Soc. A: Math. Phys. Eng. Sci. 112 (760) (1926) 151–157.
[17] J.J. Kalker, Wheel–rail rolling contact theory, Wear 144 (1–2) (1991) 243–261.
[18] H. Renondeau, Evolution des propriétés tribologiques et physico-chimiques d'une graisse polyurée dans un roulement à billes de roue (Ph.D. thesis), Ecole Centrale de Lyon, n°2004-36.
[19] M. Hoshino, Theory of grease lubrication, Jpn. J. Tribol. 47 (2002) 13–24.
[20] H.A. Spikes, The history and mechanisms of ZDDP, Tribol. Lett. 17 (3) (2004) 469–489.
[21] H. Fujita, H.A. Spikes, The formation of zinc dithiophosphate antiwear films, Proc. Inst. Mech. Eng. J: J. Eng. Tribol. 218 (4) (2004) 265–278.
[22] H. Fujita, R.P. Glovnea, H.A. Spikes, Study of zinc dialkydithiophosphate antiwear film formation and removal processes, part I: experimental, Tribol. Trans. 48 (4) (2005) 558–566.